Spin-Orbit Coupling and Interband Transitions in the Optical Conductivity of Sr_2RhO_4

Luke J. Sandilands,[1,2,5,*] Wonshik Kyung,[1,2] So Yeun Kim,[1,2] J. Son,[1,2] J. Kwon,[1,2] T. D. Kang,[1,2] Y. Yoshida,[3] S. J. Moon,[4] C. Kim,[1,2] and Tae Won Noh[1,2]

[1]*Center for Correlated Electron Systems, Institute for Basic Science, Seoul 08826, Republic of Korea*
[2]*Department of Physics and Astronomy, Seoul National University, Seoul 08826, Republic of Korea*
[3]*National Institute of Advanced Industrial Science and Technology, Tsukuba 305-8568, Japan*
[4]*Department of Physics, Hanyang University, Seoul 04763, Republic of Korea*
[5]*Measurement Science and Standards, National Research Council Canada, Ottawa, Ottawa K1A 0R6 Canada*

(Received 12 February 2017; revised manuscript received 13 July 2017; published 28 December 2017)

The prototypical correlated metal Sr_2RhO_4 was studied using optical and photoemission spectroscopy. At low energies and temperatures, the optical data reveal a complex, multicomponent response that on the surface points to an unconventional metallic state in this material. Via a comparison with photoemission, the anomalous optical response may be attributed to an unexpectedly strong interband transition near 180 meV between spin-orbit coupled bands that are nearly parallel along ΓX. This spin-orbit coupling effect is shown to occur in a number of related metallic ruthenates and explains the previously puzzling optical properties reported for these materials.

DOI: 10.1103/PhysRevLett.119.267402

Correlated electronic states in multiorbital metals are at the forefront of condensed matter physics research [1]. Metallic ruthenates are a paradigmatic class of materials in which to explore this problem. The large electronic bandwidth of these $4d$ transition metal oxides would suggest that electron-electron interactions are unimportant. On the other hand, transport measurements reveal signatures of strong correlations: the coherence scale below which Fermi liquid (FL) resistivity $\rho \propto T^2$ is observed is low and, at high T, ρ smoothly evolves into a "bad metal" state with a non-saturating $\rho \propto T$ that violates the Mott-Ioffe-Regel limit [2–4]. This apparent paradox has lead to the idea of a Hund's metal, a strongly correlated metallic state driven by Hund's coupling rather than the on-site Hubbard interaction [1,5].

In parallel with dc transport, the optical conductivity $[\hat{\sigma}(\omega) = \sigma_1(\omega) + i\sigma_2(\omega)]$ of a number of ruthenates has revealed anomalous features suggestive of strong correlation, typified by an excess of spectral weight at midinfrared frequencies ($\hbar\omega \sim 0.1$ eV) and unusual fractional power laws in $\sigma_1(\omega)$ [6–11]. These observations are in contrast with the standard theory of metals, where a rapid $1/\omega^2$ decay of $\sigma_1(\omega)$ is expected. The origin of the anomalous $\hat{\sigma}(\omega)$ and how it relates to possible non-FL states is at present an open question [12–14].

To date, the unusual $\hat{\sigma}(\omega)$ have typically been associated with the structure of the quasiparticle self-energy (i.e., scattering rate and mass enhancement) [15]. In $SrRuO_3$, for example, the $1/\sqrt{\omega}$ decay of $\sigma_1(\omega)$ has been taken as evidence for a non-FL self-energy [7,14], while in Sr_2RuO_4 the excess weight and detailed structure of $\hat{\sigma}(\omega)$ have been attributed to "resilient quasiparticles," dispersive and broad quasiparticle (QP) states predicted by dynamical mean field theory whose self-energies do not follow the FL form [10]. The notion of resilient QPs is closely linked to the issue of bad metallicity: the resilient QPs are thought to survive far above the FL coherence temperature and dominate the transport properties as the bad metallic regime is approached [16]. Crucially, these arguments rely on a single band interpretation of the optical data (i.e., the observed signal is entirely due to intraband particle-hole excitations), which may not necessarily hold at all energies [17].

In this Letter, we demonstrate that a band structure effect associated with spin-orbit coupling (SOC) leads to a strong interband contribution to $\hat{\sigma}(\omega)$ at energies $\hbar\omega \sim \lambda$, where λ is the SOC constant. This mechanism provides a natural explanation for the anomalous $\hat{\sigma}(\omega)$ and indicates a breakdown in the single-band approximation, meaning $\hat{\sigma}(\omega)$ is not associated with the QP self-energy in a straightforward way. Using optical and photoemission spectroscopies, we investigated the charge dynamics and electronic structure of Sr_2RhO_4 [18], a well-characterized and clean paramagnetic metal [21,22]. Similar to the ruthenates, the low-energy electronic structure of this material is dominated by d bands of t_{2g} symmetry, albeit accommodating one more electron [Fig. 1(a)]. Additionally, the coherent rotation of the RhO octahedra results in a $\sqrt{2} \times \sqrt{2}$ distortion. The xy-derived bands are thereby pushed completely below the Fermi level [23–25], leaving the low-energy electronic structure dominated by bands with a strong yz/xz character. Sr_2RhO_4 shows clear Fermi liquid features in photoemission [26], making it an excellent system in which to gauge the relationship between $\hat{\sigma}(\omega)$ and the underlying QP dynamics.

Despite the FL ground state in Sr_2RhO_4, our optical measurements reveal a complex, two-component charge response at low energies. In particular, a well-defined peak structure is observed in the midinfrared, which superficially

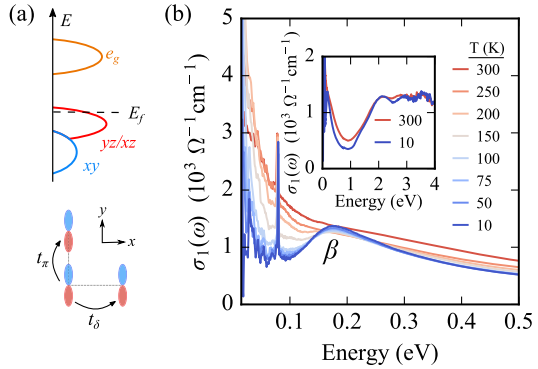

FIG. 1. (a) Top: schematic density of states near E_f. Bottom: hopping processes between yz orbitals. (b) Real part of the optical conductivity $\sigma_1(\omega)$ of Sr_2RhO_4 at different temperatures. Inset: High-energy $\sigma_1(\omega)$ at 10 and 300 K.

points to an unconventional metallic state. Via a quantitative comparison with the photoemission data, we demonstrate that the peak structure is in fact due to an unexpectedly strong, low-lying interband transition whose root cause is SOC. Although the effect of SOC on the Fermi surface is well known [27,28], its impact on $\hat{\sigma}(\omega)$ has traditionally been ignored. A comparison with the ruthenates Sr_2RuO_4 and $Ca_3Ru_2O_7$ reveals similar features, demonstrating that such SOC-activated interband transitions are common in $4d$ transition metal oxides (TMOs). We further establish that the optical self-energies extracted from an extended Drude analysis are strongly affected by the SOC-activated component, signaling a breakdown in the single-band approximation that has been widely applied in the ruthenate literature to date.

The temperature (T) dependent $\sigma_1(\omega)$ is summarized in Fig. 1(b). The $\sigma_1(\omega)$ spectra were derived over an energy range of 11 meV to 4 eV from a combination of spectroscopic reflectometry and ellipsometry [18]. At 300 K, a broad, Drude-like feature is seen at zero frequency with a shoulder near 200 meV. As T is reduced, this feature evolves into two components: a narrow QP feature centered at zero frequency and a well-defined peak (labeled β) near 180 meV. The additional sharp peak near 80 meV corresponds to an optical phonon. The inset to Fig. 1(b) shows $\sigma_1(\omega)$ over a broad energy range at 10 and 300 K. Above 0.2 eV, $\sigma_1(\omega)$ decreases down to a minimum at 0.87 eV before rising to a plateau near 2 eV associated with O p to Rh d excitations [29]. We discuss β and the QP contribution to $\sigma_1(\omega)$ in detail, starting with β.

Midinfrared peaks reminiscent of β are in fact commonly observed in the optical conductivity of strongly correlated metals and are generally interpreted as a signature of strong correlations or polaron physics [15]. The relevance of such scenarios is not, however, immediately clear in the present case. As we argue in more detail below, β may instead be traced to a low-lying interband transition that becomes optically active within the SO coupled band structure of Sr_2RhO_4, rather than exotic physics.

To substantiate the connection between β and the band structure, we apply a minimal 2D tight-binding (TB) model. The low-energy electronic structure of Sr_2RhO_4 is dominated by two quasi-1D bands derived from the yz/xz orbitals [28]. This band structure may be approximated by a TB model parametrized by three quantities: t_π, t_δ, and λ [18,28,30]. The hopping parameters t_π and t_δ describe nearest-neighbor π- and δ-type hopping processes between like orbitals [Fig. 1(a)], while λ is the SOC constant. We note that at this level of approximation the hopping is purely diagonal in the yz/xz basis, due to the symmetries of these states. SOC, on the other hand, tends to mix the yz and xz orbitals. This mixing effect is most pronounced along ΓX where, for $\lambda = 0$, the yz and xz bands are degenerate.

The TB parameters may be chosen by comparison with the angle-resolved photoemission (ARPES) data displayed in Figs. 2(a) and 2(b). Figure 2(a) shows a Fermi surface map obtained by integrating within ± 8 meV of the Fermi level (E_f). Consistent with earlier studies [23,26], the Fermi

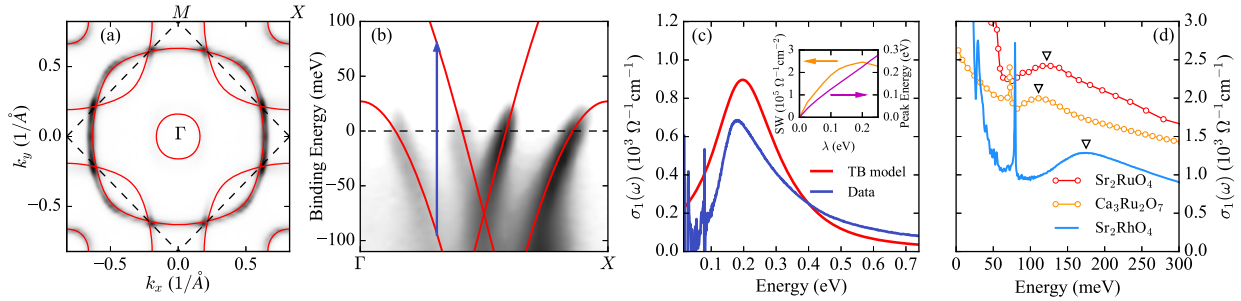

FIG. 2. (a) ARPES Fermi surface map collected at 15 K. The folded Brillouin zone is indicated with dashed lines. (b) ARPES spectra along the ΓX line. The intensity is plotted on a logarithmic scale in order to emphasize the weak back-folded bands. The TB Fermi surface and band dispersions are indicated as red lines in (a) and (b) while the dominant optical transition is indicated by a blue arrow in (b). (c) 100 K experimental and TB interband contributions to $\sigma_1(\omega)$. Inset: spectral weight (SW) and peak energy of the TB contribution vs λ. (d) Comparison of $\sigma_1(\omega)$ for Sr_2RhO_4, Sr_2RuO_4, and $Ca_3Ru_2O_7$, showing similar peak structures. The Sr_2RuO_4 and $Ca_3Ru_2O_7$ data are reproduced from Refs. [9,10] and were collected at 10 and 60 K respectively. The Sr_2RhO_4 data were collected at 100 K.

surface consists of two structures: a large electron pocket centered at Γ and a small hole pocket around X. These features are back folded by the $\sqrt{2}\times\sqrt{2}$ distortion, which takes X back to Γ, leading to additional weak structures in the ARPES data. Figure 2(b) shows a representative cut along the ΓX line. Four bands crossing E_f are visible, corresponding to the spin-orbit split yz/xz bands and their back-folded replicas. We found that the ARPES data are well described by the TB model for $(t_\pi, t_\delta, \lambda) = (0.120, 0.018, 0.172)$ eV. The TB Fermi surface and dispersions computed using these parameters are overlaid in red in Figs. 2(a) and 2(b).

With a suitable TB parametrization in hand, the interband optical conductivity $\hat{\sigma}_{\mathrm{IB}}(\omega)$ for light polarized in the x direction may be computed using the Kubo formula [31]

$$\hat{\sigma}_{\mathrm{IB}}(\omega) = i\hbar \sum_{m\neq n,\vec{k}} \frac{f_n - f_m}{\epsilon_m - \epsilon_n} \frac{\langle m,\vec{k}|\hat{j}_x|n,\vec{k}\rangle\langle n,\vec{k}|\hat{j}_x|m,\vec{k}\rangle}{\hbar\omega - (\epsilon_m - \epsilon_n) + i\eta}. \quad (1)$$

Here m and n are the band indices, $\vec{k}$ is the crystal momentum, $\hat{j}_x$ is the paramagnetic current operator, ϵ_m is the dispersion of band m, and η is a broadening parameter. The real part of $\hat{\sigma}_{\mathrm{IB}}(\omega)$ computed with Eq. (1) and setting $\eta = 0.1$ eV and $T = 0$ is shown in Fig. 2(c) and compared with the experimental β peak obtained after subtracting the QP component [18]. Despite the simplicity of our approach, the calculated conductivity agrees semiquantitatively with the data: the peak location is within 20 meV of the experimental value, while the integrated intensity agrees within ∼40%. The good agreement between our model calculation and the data strongly supports our interpretation of β as an interband transition rather than a strong correlation effect. Inclusion of a finite off-diagonal hopping term, which may be expected in $\sqrt{2}\times\sqrt{2}$ distorted Sr_2RhO_4, does not qualitatively affect the calculated $\hat{\sigma}_{\mathrm{IB}}(\omega)$ [18].

The TB analysis suggests that β is closely related to SOC. The model peak position and interband spectral weight are shown in the inset to Fig. 2(c) as a function of λ with t_π and t_δ fixed. As λ increases, the peak position increases almost linearly, while the spectral weight first increases and then saturates. This is a consequence of the symmetry of the yz/xz orbitals, which requires that electrons occupying these states may only hop between like orbitals on different sites [31]. Absent SOC, the resulting bands do not mix and the current operator $\hat{j}_x$ is purely diagonal in the yz/xz basis. In this case, no interband transitions occur. SOC, on the other hand, favors orbitally mixed total angular momentum wave functions: an upper doublet $\chi_{m_j=3/2} = (xz + iyz)\uparrow$ and $\chi_{m_j=-3/2} = (xz - iyz)\downarrow$, and a lower doublet $\chi_{m_j=1/2} = (xz + iyz)\downarrow$ and $\chi_{m_j=-1/2} = (xz - iyz)\uparrow$, where $\uparrow,\downarrow$ denotes the electron spin [28]. This effect is most pronounced along ΓX, where the yz/xz orbitals are degenerate for $\lambda = 0$, and results in nearly parallel bands of mixed yz/xz character crossing E_f and separated by $\sim\lambda$ [Fig. 2(b)]. A large number of transitions involving k points located along ΓX are therefore optically active between these SOC-split bands [arrow in Fig. 2(b)], yielding a peak structure in $\sigma_1(\omega)$ at $\hbar\omega \sim \lambda$. Because SOC plays a crucial role in this process, we refer to this situation as SOC-activated absorption.

The SOC-activated absorption mechanism is expected in other 4d TMOs with broadly similar electronic structures to Sr_2RhO_4, such as the metallic ruthenates. This is clearly seen in Fig. 2(d), where we compare the conductivity spectra of Sr_2RhO_4 with two well-studied ruthenate metals Sr_2RuO_4 and $Ca_3Ru_2O_7$ [9,10]. Similar to Sr_2RhO_4, the $\sigma_1(\omega)$ data for both ruthenate compounds reveal clear peak structures [open triangles in Fig. 2(d)] in the midinfrared. A TB analysis along the lines of Figs. 2(a)–2(c) confirms a sizable SOC-activated component for Sr_2RuO_4 and yields an estimate of $\lambda \sim 0.1$ eV, which compares well with the 0.13 ± 0.03 eV value obtained from spin-resolved photoemission [32] (see Ref. [18] for details). The SOC-activated mechanism therefore provides a natural explanation for the excess midinfrared spectral weight reported in a number of metallic ruthenates [6–11].

In the important case of Sr_2RuO_4, for example, it was recently noticed that, above ~ 0.1 eV, the $\sigma_1(\omega)$ of Sr_2RuO_4 is significantly larger than expected from simple FL theory [10]. This was interpreted as evidence for the resilient QP scenario: resilient QPs are expected to have velocities larger than the bare dispersion and should manifest themselves as excess spectral weight in $\sigma_1(\omega)$ [10]. Our results suggest that this picture should be reexamined as the excess spectral weight near 0.1 eV is likely associated, at least in part, with SOC-activated interband absorption.

Two other ruthenate metals whose optical properties have attracted significant attention are $SrRuO_3$ and $CaRuO_3$. At the lowest energies and temperatures, these materials are FLs [33,34]. The optical conductivity, however, is highly unusual: non-FL scaling is observed and $\sigma_1(\omega)$ decays as $1/\sqrt{\omega}$, slower than the conventional $1/\omega^2$ FL dependence [7,8,35]. On the surface, these features indicate a breakdown of FL theory at these energies [14,36]. Dang *et al.* have identified low-lying interband transitions associated with the $GdFeO_3$-type distortion as the source of the apparent non-FL features at terahertz frequencies [17]. We expect that the SOC-activated mechanism treated in our work plays a similar role at energies $\hbar\omega \sim 0.1$ eV.

Having discussed the interband contribution to $\hat{\sigma}(\omega)$, we now focus on the zero energy peak [Fig. 1(b)], which reflects the QP dynamics. We used a phenomenological Drude-Lorentz (DL) model to subtract the interband contribution to $\hat{\sigma}(\omega)$ and isolate the QP component. The spectra were fit to a DL model that includes two Drude terms for the QP component, a Lorentzian for the phonon near 80 meV, two Lorentzians for the SOC-activated interband contribution, and an additional Lorentzian

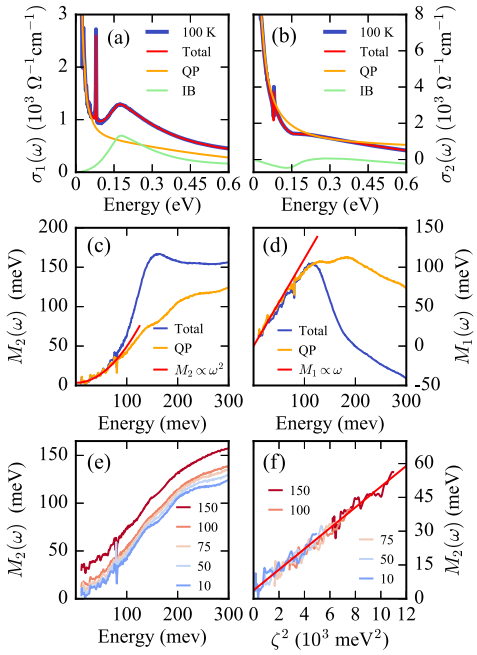

FIG. 3. Fermi liquid electrodynamics of Sr_2RhO_4: [(a) and (b)] Drude-Lorentz (DL) decomposition of $\hat{\sigma}(\omega)$ at 100 K. [(c) and (d)] $\hat{M}(\omega)$ at 10 K with $\hbar\omega_p = 2.1$ eV. (e) $M_2^q(\omega)$ at various temperatures. (f) FL scaling of $M_2^q(\omega)$ with $\zeta^2 = (\hbar\omega)^2 + b(\pi k_b T)^2$ and $b = 3.6$.

located near 2 eV that accounts for the high-energy O $2p$ to Rh $4d$ charge transfer excitations. A representative fit is shown in Figs. 3(a) and 3(b). From the spectral weight of the Drude oscillators, we estimate a free carrier plasma frequency $\hbar\omega_p = 2.1$ eV. Details of the DL model may be found in Ref. [18].

Insight into the QP dynamics is often obtained through the extended Drude analysis. In this approach $\hat{\sigma}(\omega)$ is recast in terms of a complex memory function $\hat{M}(\omega) = M_1(\omega) + iM_2(\omega)$ defined as [15]

$$\hat{\sigma}(\omega) = \frac{i\epsilon_o\omega_p^2}{\omega + \hat{M}(\omega)}. \tag{2}$$

Here ω_p is the plasma frequency and ϵ_o is the permittivity of free space. In the single-band limit, $M_2(\omega)$ is the scattering rate of particle-hole pair excitations, while $M_1(\omega)$ is related to the QP mass enhancement via $m^*(\omega)/m = 1 + M_1(\omega)/\omega$ [15]. For a local FL, $\hat{M}(\omega) = [1/\tilde{Z} - 1]\hbar\omega + iA[(\hbar\omega)^2 + b(\pi k_b T)^2]$, where the thermal factor $b = 4$ and $\tilde{Z}$ is proportional to the QP weight Z [10,37,38].

The memory function at 10 K obtained from the QP component $[\hat{M}^q(\omega)]$ is shown in Figs. 3(c) and 3(d). At low energies, $M_2^q(\omega)$ $[M_1^q(\omega)]$ rises quadratically (linearly) with energy, as expected for a FL metal [38]. A linear fit to $M_1^q(\omega)$ implies $m^*(\omega)/m \sim 2.1$ or $\tilde{Z} \sim 0.48$. This figure is consistent with a LDA + DMFT study that found a (band-dependent) Z of 0.5–0.6 [24] and also with the renormalization of the experimental electronic specific heat ($\gamma_{\text{exp}}/\gamma_{\text{theory}} \sim 2.2$) and cyclotron masses ($m_{\text{exp}}/m_{\text{theory}} \sim 2.1$ to 2.3) relative to density functional theory [28]. Above 75 meV, $\hat{M}^q(\omega)$ begins to deviate from the FL form: $M_2(\omega)$ increases slower than ω^2 before gradually saturating, while $M_1(\omega)$ reaches a weak maximum near 200 meV before decreasing.

The T dependence of the $M_2^q(\omega)$ data is also consistent with FL theory. As shown in Fig. 3(e), $M_2(\omega)$ increases rigidly as T is raised, with the low-energy ω^2 behavior preserved. Indeed, for $T \leq 150$ K and $\hbar\omega \leq 75$ meV the data may be collapsed onto an effective FL form $M_2(\omega, T) = \Gamma_0 + A[\hbar\omega^2 + b(\pi k_b T)^2] = \Gamma_0 + A\zeta^2$ with $\Gamma_0 = 3.5$ meV, $A = 4.7 \times 10^{-3}$ meV^{-1}, and $b = 3.6$ [Fig. 3(f)]. FL scaling with $b = 4$ is in fact rarely observed: most materials examined to date also reveal $b \neq 4$ [37,39]. The fact that $b \neq 4$ in the present case may be due to a residual interband contribution not properly accounted for by our DL analysis or an added elastic scattering channel [37]. Given the multiband Fermi surface of Sr_2RhO_4 [Fig. 2(a)], it is not obvious that $M_2(\omega, T)$ should follow the FL form. The success of the effective single-component FL scaling analysis therefore suggests that the self-energies of the bands at E_f are similar, in line with the relatively band-independent mass enhancements found in LDA + DMFT and in quantum oscillation experiments [24,28], and that intraband excitations dominate at low energies.

For $\hbar\omega \sim \lambda$, the extended Drude analysis is strongly affected by the SOC-activated absorption. This may be seen in Figs. 3(c) and 3(d) where we compare $\hat{M}(\omega)$ computed from the total conductivity $[\hat{M}^t(\omega)]$ and $\hat{M}^q(\omega)$. At low energies, the two cases are quite similar. Above 60 meV, however, the two cases differ markedly: $M_2^t(\omega)$ increases more rapidly than ω^2 and reaches a maximum near 150 meV before saturating, while $M_1^t(\omega)$ shows a sharp change of slope near 100 meV followed by a rapid decrease. We found that at low energies ($\hbar\omega \leq 60$ meV), the $M_2^t(\omega, T)$ data may still be described with an effective FL form, albeit with quantitatively different $b = 3$ [Fig. S4 of Ref. [18]]. An interesting question is therefore whether unresolved interband contributions to $\hat{\sigma}(\omega)$ may be behind the $b \neq 4$ reported for a number of other materials [39]. Finally, we also note that, in the ruthenate literature, the optical self-energies extracted from an extended Drude analysis have often been taken as evidence for unconventional metallic states (e.g., Refs. [7,10]). Figures 3(c) and 3(d) indicate that such arguments may need to be reconsidered, as the total $\hat{\sigma}(\omega)$ is not related to the QP self-energy in the simple manner of Eq. (2).

To recap, Sr_2RhO_4 has been studied with optical and photoemission spectroscopy. The optical data reveal a complex low-energy response, including a midinfrared peak

structure. Through a comparison with photoemission, we demonstrated that this peak may be traced to a band structure effect associated with strong SOC. This SOC-activated absorption mechanism is a common feature of 4*d* TMOs with broadly similar electronic structures to Sr_2RhO_4 and may also lead to strong magneto-optical effects [40].

This work was supported by the Institute for Basic Science in Korea Grant No. IBS-R009-D1 and IBS-R009-G2. S. J. M. was supported by Basic Science Research Program through the National Research Foundation of Korea funded by the Ministry of Science, ICT and Future Planning (Grants No. 2014R1A2A1A11054351 and No. 2017R1A2B4009413).

*Corresponding author.
Luke.Sandilands@nrc-cnrc.gc.ca

[1] A. Georges, L. d. Medici, and J. Mravlje, Annu. Rev. Condens. Matter Phys. **4**, 137 (2013).
[2] A. W. Tyler, A. P. Mackenzie, S. NishiZaki, and Y. Maeno, Phys. Rev. B **58**, R10107 (1998).
[3] J. Bruin, H. Sakai, R. Perry, and A. Mackenzie, Science **339**, 804 (2013).
[4] P. B. Allen, H. Berger, O. Chauvet, L. Forro, T. Jarlborg, A. Junod, B. Revaz, and G. Santi, Phys. Rev. B **53**, 4393 (1996).
[5] L. de' Medici, J. Mravlje, and A. Georges, Phys. Rev. Lett. **107**, 256401 (2011).
[6] A. V. Puchkov, M. C. Schabel, D. N. Basov, T. Startseva, G. Cao, T. Timusk, and Z.-X. Shen, Phys. Rev. Lett. **81**, 2747 (1998).
[7] P. Kostic, Y. Okada, N. C. Collins, Z. Schlesinger, J. W. Reiner, L. Klein, A. Kapitulnik, T. H. Geballe, and M. R. Beasley, Phys. Rev. Lett. **81**, 2498 (1998).
[8] Y. S. Lee, J. Yu, J. S. Lee, T. W. Noh, T.-H. Gimm, H.-Y. Choi, and C. B. Eom, Phys. Rev. B **66**, 041104 (2002).
[9] J. S. Lee, S. J. Moon, B. J. Yang, J. Yu, U. Schade, Y. Yoshida, S.-I. Ikeda, and T. W. Noh, Phys. Rev. Lett. **98**, 097403 (2007).
[10] D. Stricker, J. Mravlje, C. Berthod, R. Fittipaldi, A. Vecchione, A. Georges, and D. van der Marel, Phys. Rev. Lett. **113**, 087404 (2014).
[11] C. Mirri, F. M. Vitucci, P. Di Pietro, S. Lupi, R. Fittipaldi, V. Granata, A. Vecchione, U. Schade, and P. Calvani, Phys. Rev. B **85**, 235124 (2012).
[12] S. Acharya, M. S. Laad, D. Dey, T. Maitra, and A. Taraphder, Sci. Rep. **7**, 43033 (2017).
[13] Z. P. Yin, K. Haule, and G. Kotliar, Phys. Rev. B **86**, 195141 (2012).
[14] P. Werner, E. Gull, M. Troyer, and A. J. Millis, Phys. Rev. Lett. **101**, 166405 (2008).
[15] D. N. Basov, R. D. Averitt, D. van der Marel, M. Dressel, and K. Haule, Rev. Mod. Phys. **83**, 471 (2011).
[16] X. Deng, K. Haule, and G. Kotliar, Phys. Rev. Lett. **116**, 256401 (2016).
[17] H. T. Dang, J. Mravlje, A. Georges, and A. J. Millis, Phys. Rev. Lett. **115**, 107003 (2015).
[18] See Supplemental Material at http://link.aps.org/supplemental/10.1103/PhysRevLett.119.267402 for experimental methods and details of the data analysis, which includes Refs. [19,20].
[19] C. C. Homes, M. Reedyk, D. Cradles, and T. Timusk, Appl. Opt. **32**, 2976 (1993).
[20] A. Kuzmenko, Rev. Sci. Instrum. **76**, 083108 (2005).
[21] R. S. Perry, F. Baumberger, L. Balicas, N. Kikugawa, N. J. C. Ingle, A. Rost, J. F. Mercure, Y. Maeno, Z. X. Shen, and A. P. Mackenzie, New J. Phys. **8**, 175 (2006).
[22] I. Nagai, N. Shirakawa, N. Umeyama, and S.-I. Ikeda, J. Phys. Soc. Jpn. **79**, 114719 (2010).
[23] B. J. Kim, J. Yu, H. Koh, I. Nagai, S. I. Ikedaa, S.-J. Oh, and C. Kim, Phys. Rev. Lett. **97**, 106401 (2006).
[24] C. Martins, M. Aichhorn, L. Vaugier, and S. Biermann, Phys. Rev. Lett. **107**, 266404 (2011).
[25] K.-H. Ahn, K.-W. Lee, and J. Kunes, J. Phys. Condens. Matter **27**, 085602 (2015).
[26] F. Baumberger, N. J. C. Ingle, W. Meevasana, K. M. Shen, D. H. Lu, R. S. Perry, A. P. MacKenzie, Z. Hussain, D. J. Singh, and Z.-X. Shen, Phys. Rev. Lett. **96**, 246402 (2006).
[27] M. W. Haverkort, I. S. Elfimov, L. H. Tjeng, G. A. Sawatzky, and A. Damascelli, Phys. Rev. Lett. **101**, 026406 (2008).
[28] G.-Q. Liu, V. N. Antonov, O. Jepsen, and O. K. Andersen, Phys. Rev. Lett. **101**, 026408 (2008).
[29] S. J. Moon, M. W. Kim, K. W. Kim, Y. S. Lee, J.-Y. Kim, J.-H. Park, B. J. Kim, S.-J. Oh, S. Nakatsuji, Y. Maeno, I. Nagai, S. I. Ikeda, G. Cao, and T. W. Noh, Phys. Rev. B **74**, 113104 (2006).
[30] J.-M. Carter, V. Shankar, and H.-Y. Kee, Phys. Rev. B **88**, 035111 (2013).
[31] M. Xie, G. Khalsa, and A. H. MacDonald, Phys. Rev. B **89**, 245417 (2014).
[32] C. N. Veenstra, Z.-H. Zhu, M. Raichle, B. M. Ludbrook, A. Nicolaou, B. Slomski, G. Landolt, S. Kittaka, Y. Maeno, J. H. Dil, I. S. Elfimov, M. W. Haverkort, and A. Damascelli, Phys. Rev. Lett. **112**, 127002 (2014).
[33] A. P. Mackenzie, J. W. Reiner, A. W. Tyler, L. M. Galvin, S. R. Julian, M. R. Beasley, T. H. Geballe, and A. Kapitulnik, Phys. Rev. B **58**, R13318 (1998).
[34] M. Schneider, D. Geiger, S. Esser, U. S. Pracht, C. Stingl, Y. Tokiwa, V. Moshnyaga, I. Sheikin, J. Mravlje, M. Scheffler, and P. Gegenwart, Phys. Rev. Lett. **112**, 206403 (2014).
[35] J. S. Dodge, C. P. Weber, J. Corson, J. Orenstein, Z. Schlesinger, J. W. Reiner, and M. R. Beasley, Phys. Rev. Lett. **85**, 4932 (2000).
[36] M. S. Laad and E. Müller-Hartmann, Phys. Rev. Lett. **87**, 246402 (2001).
[37] D. L. Maslov and A. V. Chubukov, Phys. Rev. B **86**, 155137 (2012).
[38] C. Berthod, J. Mravlje, X. Deng, R. Žitko, D. van der Marel, and A. Georges, Phys. Rev. B **87**, 115109 (2013).
[39] U. Nagel, T. Uleksin, T. Rõõm, R. P. S. M. Lobo, P. Lejay, C. C. Homes, J. S. Hall, A. W. Kinross, S. K. Purdy, T. Munsie, T. J. Williams, G. M. Luke, and T. Timusk, Proc. Natl. Acad. Sci. U.S.A. **109**, 19161 (2012).
[40] T. Tanaka and H. Kontani, Phys. Rev. B **77**, 195129 (2008).